Journal of Marine Research, 43, 517–539, 1985

Correlation scales, objective mapping and a statistical test of geostrophy over the continental shelf

by Kenneth L. Denman[1] and Howard J. Freeland[1]

ABSTRACT

We have constructed spatial structure functions for oceanographic variables, collected during 15 cruises off the coast of Vancouver Island, Canada over a 3 year period (1979–81), to determine the appropriate correlation function and unresolved noise level for objective mapping according to the Gauss-Markov theorem. The assumption of quasigeostrophic flow has been tested by comparing the longitudinal and transverse velocity shear structure functions derived from geopotential height fields with those derived from 6 current meter moorings. In addition objective maps of geopotential height imply current shears similar to the directly observed shear vectors, as would be expected under geostrophic control. Structure functions of geopotential height, temperature, salinity, and log-transformed phytoplankton chlorophyll *a* pigment concentration all have a broad maximum near a separation of 30 km, consistent with a dominant eddy wavelength of ≃60 km, also the estimated wavelength of the most unstable baroclinic disturbance. The sensitivity of the objective maps generated using the Gauss-Markov theorem to different correlation functions, length scales and noise levels was tested: where the sampling was well distributed, the patterns changed little.

Temporal structure functions (for data from 25 cruises) of geopotential height, temperature and salinity are roughly cyclic with minima at time lags of 1 and 2 years. The structure functions increase monotonically with lags up to at least 90 days indicating that temporal changes during a ship survey (several days) are sufficiently small that the maps can be regarded as synoptic. Finally, a composite kinetic energy spectrum from a long term (≃3 years) current meter mooring at the edge of the continental shelf has well defined peaks in a band with 10–50 day periods (which we believe represents the mesoscale eddies with ≃60 km wavelength), and at the annual and the major tidal and inertial periods.

1. Introduction

Objective mapping techniques have been used on open ocean data for at least a decade to construct two-dimensional maps of oceanographic variables (e.g., Freeland and Gould, 1976; McWilliams, 1976). However, they have not been widely used over continental shelves because there the fields of velocity and scalar variables are known to be inhomogeneous, anisotropic and nonstationary. In this paper, we examine, for a region over the continental shelf, the robustness of two-dimensional maps prepared

1. Institute of Ocean Sciences, P. O. Box 6000, Sidney, BC, Canada, V8L 4B2.

with an objective technique that incorporates our knowledge of the spatial and temporal scales of mesoscale patterns and of the magnitude of unresolved variability.

Objective analysis using the Gauss-Markov theorem provides one rational technique for fitting in a least squares sense the 'optimal' mapping surface to a set of observations. One's prior knowledge and assumptions are made explicit and are quantified regarding: the scales of correlation and hence of spatial interpolation, and the magnitude of small scale uncertainty resulting from sampling errors and from unresolved structure associated with internal waves, small eddies, fronts, etc. The technique provides, in addition to the optimally fitted maps, an estimate of unresolved variability in the observations and an expected error map for a given sampling grid, based on assumptions of homogeneity, isotropy and stationarity. Also, our application of the Gauss-Markov theorem employing structure functions allows us to test the consistency of the assumption of geostrophic flow with our data set.

In this paper, we analyze current meter data from 6 moorings and hydrographic data from 25 cruises, all obtained over a 3 year period (1979–81) from the continental shelf region off southwest Vancouver Island, British Columbia. First, we estimate the spatial autocovariance function from structure functions of the geopotential difference between two reference depths determined from the hydrographic data, from which longitudinal and transverse velocity shear structure functions can be obtained by differentiation of the fitted function. These are compared directly with velocity structure functions formed from velocity measurements made with current meters on different moorings to test statistically the hypotheses of homogeneous geostrophic turbulent flow. Autocorrelation functions for near-surface temperature, salinity and phytoplankton chlorophyll *a* pigment concentration (derived from fluorescence) are then determined from structure functions, and various maps are generated to demonstrate the pattern sensitivity to our choice of correlation function (shape and averaging distance) and of noise level. Temporal structure functions are calculated to test our assumption of synopticity during a single survey and to determine the time scales of fluctuation in each variable. Finally, we have used the spatial structure functions, a time series of internal Rossby radius of deformation, and a kinetic energy spectrum of currents measured at a long term mooring to infer characteristic space and time scales for mesoscale patterns in the sampling area.

2. Theory

a. Objective analysis of scalar fields. The basic theory of objective analysis employing the Gauss-Markov theorem was first widely used in the preparation of meteorological synoptic maps. We follow the formulation of Gandin (1965) and its introduction to oceanography by Bretherton *et al.* (1976). Particularly readable accounts of its use are Alaka and Elvander (1972) and Karweit (1980).

For a scalar field, the general problem is to compute an estimate $\hat{\theta}(\mathbf{x})$ of the value $\theta(\mathbf{x})$ of a scalar variable at any position $\mathbf{x} = (x, y)$ from inexact observations ϕ_n of the

variable at a limited number of data positions $\mathbf{x}_n$, $(n = 1,2, \ldots, N)$. We use the Gauss-Markov theorem to obtain (following Bretherton *et al.*, 1976; Bretherton and McWilliams, 1980) the optimum linear estimator for $\theta(\mathbf{x})$. Its implementation requires *a priori* knowledge for an area of a variable's covariance $F(\mathbf{r})$ and uncorrelated error variance E, where $\mathbf{r}$ is the vector separation between positions. When choosing suitable functional forms of F, we apply two constraints (e.g., Yaglom, 1962). First, $\partial^2 F/\partial x^2$ and $\partial^2 F/\partial y^2$ must be continuous at $|\mathbf{r}| = 0$; otherwise we are not dealing with a continuously differentiable process, but rather a Markov-like process. Second, the variance spectrum derived from $F(\mathbf{r})$ must be integrable and non-negative for all wavenumbers $\mathbf{k}$: otherwise, we are not dealing with a realizable stochastic random process. The second constraint implies that $F \to 0$ when $|\mathbf{r}| \gg L_d$, where L_d is some natural length scale of the field being sampled; in this case the local internal Rossby radius of deformation seems appropriate. We found our data insufficient to resolve the anisotropy of the covariance function known to exist especially at scales comparable to and greater than the shelf width, and have replaced $F(\mathbf{r})$ by an isotropic function which we write here as $F(r)$, where $r = |\mathbf{r}|$.

As an alternative to estimating $F(r)$ from data pairs, we chose to use the structure function

$$\begin{aligned} G(r) &= \langle(\theta(\mathbf{x} + \mathbf{r}) - \theta(\mathbf{x}))^2\rangle, \qquad (r = |\mathbf{r}|) \\ &= \langle\theta(\mathbf{x} + \mathbf{r})\theta(\mathbf{x} + \mathbf{r})\rangle + \langle\theta(\mathbf{x})\theta(\mathbf{x})\rangle - 2\langle\theta(\mathbf{x} + \mathbf{r})\theta(\mathbf{x})\rangle \\ &= 2\,[F(0) - F(r)]. \end{aligned} \tag{1}$$

The structure function $B(r)$, formed from observations, is increased by an amount $2E$

$$\begin{aligned} B(r) &= G(r) + 2E \\ &= 2\,[F(0) + E - F(r)] \\ &= 2E + 2F(0)[1 - R(r)] \end{aligned} \tag{2}$$

where $R(r) = F(r)/F(0)$ is the noise-free autocorrelation function with properties $R(0) = 1$ and $R(r) \to 0$ as $r \to \infty$. The advantages of using the structure function are that it does not require explicit use of a mean, and the noise variance E can be estimated independently of the signal variance $F(0)$. Finally, for a two-dimensional isotropic field, $S(k)$ the band averaged power spectrum (as a function of scalar wavenumber k), is obtained by a Hankel transform of the covariance function $F(r)$ (Gandin, 1965):

$$S(k) = \int_0^\infty rF(r)\, J_0(kr)dr. \tag{3}$$

b. Analysis of the stream function field. We wish to test the consistency of the hydrographic data with the geostrophic assumption by a statistical comparison between the stream function field and measurements made from current meters. Relationships can be derived (see Monin and Yaglom, 1975) between structure

functions of geopotential height and current speed that are analogous to relationships between correlation functions presented by Bretherton *et al.* (1976).

For an isotropic velocity field, structure functions of velocity can be expressed in terms of the longitudinal and transverse two point scalar structure functions $D_L(r)$ and $D_T(r)$. For a nondivergent velocity field, the structure function of the streamfunction, $B_\psi(r) = \langle(\psi(\mathbf{x}) - \psi(\mathbf{x} + \mathbf{r}))^2\rangle$, is related to the scalar structure functions $D_L(r)$ and $D_T(r)$ (to within a constant of integration) in the following manner for two dimensions:

$$D_L(r) = -(1/r)dB_\psi/dr \tag{4a}$$

$$D_T(r) = -d^2B_\psi/dr^2. \tag{4b}$$

If we assume further that the flow is quasi-geostrophic, then the streamfunction is Φ/f where Φ is the geopotential height (in $J\ kg^{-1}$) between two reference depths $z_1 > z_2$ (z positive upwards), and f ($= 2\Omega \sin \lambda$) is the local (constant) inertial frequency (in s^{-1}). Note that Φ (in $J\ kg^{-1}$) $= 10\Delta D$ (in dynamic meters). The calculated velocities u and v are thus the velocity components of the fluid at depth z_1 relative to z_2 at $\mathbf{x}$ or $\mathbf{x} + \mathbf{r}$, and $D_L(r)$ and $D_T(r)$ calculated from Eq. (4) represent derived structure functions of those (assumed geostrophic) velocities at $\mathbf{x}$ and $\mathbf{x} + \mathbf{r}$. Completely independent estimates of $D_L(r)$ and $D_T(r)$ can be obtained from current meters at z_1 and z_2 on moorings at different positions separated by a distance r, and compared with the functions obtained from the hydrographic data, thereby providing a statistical test of the consistency of the data with the hypothesis that the flow is quasi-geostrophic.

3. Calculations of spatial structure functions

a. Detrending the data. We collected data from the area off southwestern Vancouver Island shown in Figure 1 on 25 cruises during the period from January 1979 to September 1981. On some cruises only a line of stations along the southern line of current meter moorings was sampled. Structure functions were estimated for geopotential height between 50 and 100 m depths and for temperature and salinity (average over 0 to 5 m) for data from 15 cruises that had adequate two-dimensional coverage. Two of the cruises were split into two surveys each to give a similar areal coverage and similar survey time for all data sets, and to minimize temporal changes occurring during any one survey. Chlorophyll pigment concentrations were calculated from *in situ* fluorescence profiles (integrated over the depth range 0–50 m), and structure functions were calculated for data from eight surveys during six cruises.

In data collected from a continental shelf region, trends and inhomogeneities are almost certain to occur, especially in the onshore-offshore direction. In particular, a mean geostrophic current requires a linear trend in geopotential height, resulting in a quadratic term in either the structure function or covariance function formed from the geopotential height field. We found that the structure functions for both geopotential

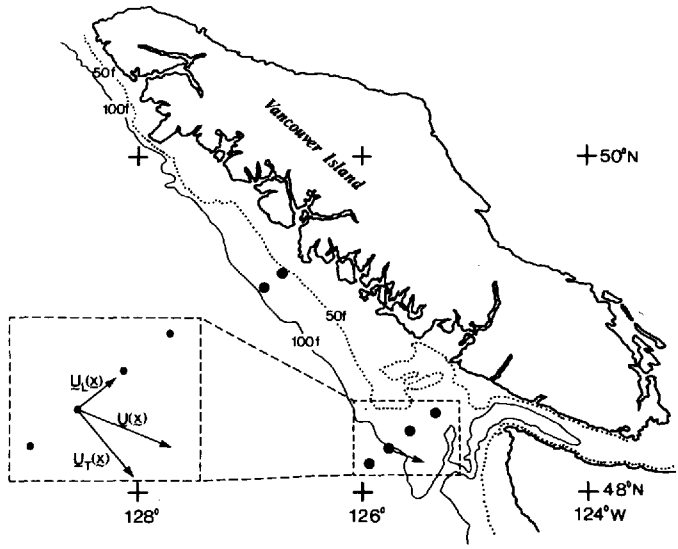

Figure 1. Location of the cruises off Vancouver Island, British Columbia. Sample current vectors at each mooring are shown resolved into longitudinal (U_L) and transverse (U_T) components for structure function analysis. Bottom contours are in fathoms (100 fm = 183 m).

height and temperature were dominated by this quadratic term. To minimize the effect of large scale trends and to concentrate on mesoscale patterns, we then tried fitting a plane in (x, y, t) space to the data from each cruise and performing the analysis on the residuals about the plane. The fit on time t, which would remove any linear change in the whole field during the course of a single survey (2–4 days), was never significant; thus only an (x, y) plane was fitted and removed from the data from each survey. Because large scale curvilinear trends are not removed by a least squares fitted plane, $F(r)$ may still be poorly determined for each cruise, often not approaching zero with increasing separation.

The optimal linear estimates obtained with the Gauss-Markov technique are also the maximum likelihood estimates provided that the hypothesis of a normally distributed parent population is roughly valid (Mood and Graybill, 1963). However, distributions of plankton are seldom normal (e.g., Cassie, 1963), and phytoplankton chlorophyll estimated from satellite is distributed roughly logarithmically (Smith and Baker, 1982). The combination of a logarithmic transformation and (x, y) plane removal reduced the number of chlorophyll surveys that were non-normal from 7 of 8 to only 2. [To determine which surveys were non-normal we used the Kolmogorov-Smirnov test statistic at the 95% confidence level, modified for the case where the mean and variance are estimated from the sample population after Kendall and Stuart (1979), and Lilliefors (1967).] The linear plane was removed from the salinity and the

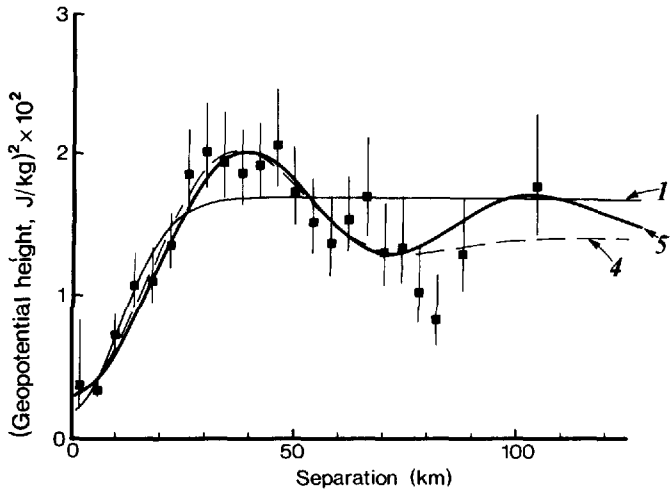

Figure 2. Spatial structure functions of geopotential height. The solid squares are estimates from the CTD station data, and the numbered lines are fitted functions (see text and Table 1). The light solid line is R_1, the dashed line is the best fit statistically (R_4), and the heavy solid line is the best fit of a realizable function (R_5). The vertical bars represent relative 95% confidence regions for a χ^2 variable. See text for details.

transformed chlorophyll data so that all four variables were treated the same. While other curvilinear trend removal algorithms are possible, the quadratic nature of the original structure functions formed from geopotential height and temperature data made the removal of an (x, y) plane the most obvious choice.

b. Binned estimates and fitted functions. We have calculated, for each increment in spatial separation of 4 km, a single structure function estimate from all data pairs whose spatial separation fell within that increment or bin. Raw estimates are χ^2 variables with a very low number of degrees of freedom (df), but we require binned estimates with a larger df so that we can fit functional forms of $F(r)$ by least squares analysis (see also Mackas, 1984). Because of large differences between surveys in the signal levels of temperature, salinity and chlorophyll (but not geopotential height), the bin estimates from each survey for those variables were divided by twice the variance for that survey before overall averages were formed.

Plotted in Figure 2 are the weighted average (over 17 surveys) bin estimates of the structure function of geopotential height between the depths of 50 and 100 m. As the structure function is a χ^2 random variable (even at small separations r where the data are correlated, under the hypothesis of joint normality), relative 95% confidence limits for a χ^2 variable have been calculated and plotted for each bin estimate based only on the number of data pairs in that bin. Correlation between neighboring data pairs (Bretherton *et al.*, 1976; Bretherton and McWilliams, 1980) has not been considered,

but for our sampling grids the *df* would probably be reduced proportionately in all bins. The binned structure function estimates for geopotential height residuals shown in Figure 2 clearly do not increase monotonically with increasing separation. Rather a maximum occurs at separations around 30 km followed by a slow decrease approaching a constant asymptote with increasing r.

To obtain a functional form for $F(r)$ to use in the objective mapping algorithm, we have fitted several forms of Eq. (2) to the data in Figure 2 with a weighted nonlinear least squares procedure using the Marquardt algorithm (Bevington, 1969). The relative weights used were derived from the *df* based on the number of pairs of data points in each bin estimate without regard for covariability of neighboring data pairs. However, the fits changed insignificantly when the weights were all set equal or when they varied randomly over a factor of 2. The results for 5 possible expressions for $R(r)$, all of which have second derivatives at $r = 0$, are summarized in Table 1, and 3 of them are plotted in Figure 2. For the function R_1 we fit $F(0)$, E and the coefficients in $R_i(r)$; for subsequent functions E was estimated by eye, and only the other coefficients were fitted.

The function $R_1 = \exp(-r^2/a^2)$, despite its simplicity and computational efficiency, fits only the initial portion of the calculated estimates. R_2 and R_4 fit the data well, but their spectra calculated from Eq. (3) were negative at low wave numbers for the values of a and b obtained by least squares fitting. R_5 does have a realizable positive definite spectrum however, it fits our data well, and it produces stable realistic objective maps. The functions $R_i (i = 2, \ldots, 5)$ all have a spectral peak, the limiting case being the obviously unrealistic Bessel function R_3, which has a delta function spectrum.

We have plotted in Figure 3 the longitudinal and transverse velocity structure functions $D_L(r)$ and $D_T(r)$ calculated from Eq. (4) with the fitted correlation function R_5 for comparison with the values (solid circles) calculated from various pairs of the moorings at positions shown in Figure 1. The current meter data were first filtered with a Lanczos-cosine filter with a half power point at 39 hours. (This filter effectively eliminates internal tides and other short term fluctuations.) Then, at each mooring, the instantaneous current at 100 m was subtracted from that at 50 m to form a current shear to compare with the geostrophic current. Each data point represents a cumulative record length of between 301 and 580 days. The 90% confidence intervals were calculated for a χ^2 variable with 1 *df* for each 10 days of record (consistent with mesoscale spectral peak in kinetic energy at a 20 day period in Fig. 11).

The functions $D_L(r)$ and $D_T(r)$ have not been scaled or normalized to fit the values calculated from the observed currents, but are plotted in physical units. The longitudinal structure functions agree in absolute magnitude of the signal variance (the large separation asymptote) giving some confidence in the trend removal procedure. However, the measured current shear differences increase more rapidly with increasing distance than do those inferred from the geopotential height field, possibly because the separations were all across the continental shelf in the direction of maximum

Table 1. Functional forms of the autocorrelation function $R_i(r)$ used in fits to structure function estimates of geopotential height. All functions have continuous derivatives at $r = 0$ and their ring-averaged spectra $S(k)$ are shown in the table. The lowest χ^2 value represents the best fit (not adjusted for different numbers of fitted coefficients).

		Fitted Coefficients					
i	R_i	a (km)	b (km)	#	χ^2	$S_i(k) = \int_0^\infty R_i(r)J_0(kr)rdr$	Comments
1	$\exp(-r^2/a^2)$	15.2	—	3*	0.0152	$\exp(-a^2k^2/4)$	Good spectral behavior; peak at $k = 0$.
2	$\exp(-r^2/a^2)(1 - r^2/b^2)$	30.4	19.0	3	0.0055	$[1 - a^2/b^2 + ka^3/(2b^2)]S_1(k)$	$S_2(k)$ + *ve* for $a < b$; goes − *ve* for $a > b$.
2a	(R_2 with $a = b$)	24.4	—	2	0.0100	$akS_1(k)/2$	$S_{2a}(0) = 0$, + *ve* elsewhere.
3	$J_0(r/a)$	10.3	—	2	0.0073	$\delta(k - 1/a)$	Plane wave solution.
4	$\exp(-r^2/a^2)\cos(r/b)$	51.8	20.9	3	0.0051	(solved numerically)	Spectrum − *ve* at small k when $a/b > 1.848$ (fitted $a/b = 2.47$).
5	$\exp(-r^2/a^2)\,J_0(r/b)$	124	10.3	3	0.0060	$\exp[-a^2(1 + b^2k^2)/(4b^2)]$ · $I_0[a^2k/(2b)]$ [@]	Spectrum + *ve* everywhere but narrow peak for large a.

*the noise value E is also fitted.

[@] I_0 is the modified Bessel function.

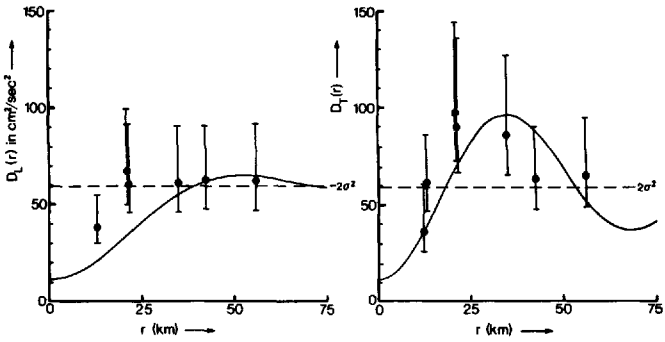

Figure 3. Longitudinal and transverse velocity structure functions. The smooth curves are derived from function 5 using Eqs. (4) (shown in Fig. 2), and the solid circles are estimates calculated from pairs of moorings in Figure 1. Relative confidence regions are indicated as in Figure 2.

gradient in bottom depth. There was reasonable agreement in both the absolute magnitude and the general shape of the transverse structure functions providing some confidence in our hypothesis of nondivergent quasi-geostrophic flow (for the depth interval 50 to 100 m). We expect, therefore, that objective maps of geopotential height computed using our fitted covariance function will show good agreement with observed low-pass filtered shear measurements from current meter moorings. Although our station sampling scheme was directionally biased with smaller spacing between stations across the shelf and larger spacings along the shelf, separating station pairs into across shelf and along shelf directions did not produce clear differences in the resulting directional structure functions. Hence, all results reported here assume directional isotropy, although a larger data set should resolve the directional anisotropy commonly believed to exist over continental shelves.

Binned structure function estimates for temperature, salinity and log-transformed chlorophyll are shown in Figure 4. All three possess a broad peak near a separation of 30 km, as did geopotential height, but the drop-off for greater separations is less pronounced in chlorophyll. The similarity of these functions to that for geopotential height between 50 and 100 m depth suggests that advection by the flow field controls the horizontal mesoscale patterns of near-surface scalar variables. This result is not expected *a priori* for chlorophyll, which is a passive scalar but not conserved in the sense that spatial patterns can arise from either production of biomass by photosynthesis or loss of biomass through grazing by zooplankton (e.g. Bennett and Denman, 1985). This statistical similarity in mesoscale pattern implies that, at those scales, either variations in the height of density surfaces control variations in the geopotential height field and in the availability of nutrients, with the result that chlorophyll patterns are correlated with eddies in the flow field, or the growth and loss processes acting on the phytoplankton have little effect on the horizontal patterns in their distributions.

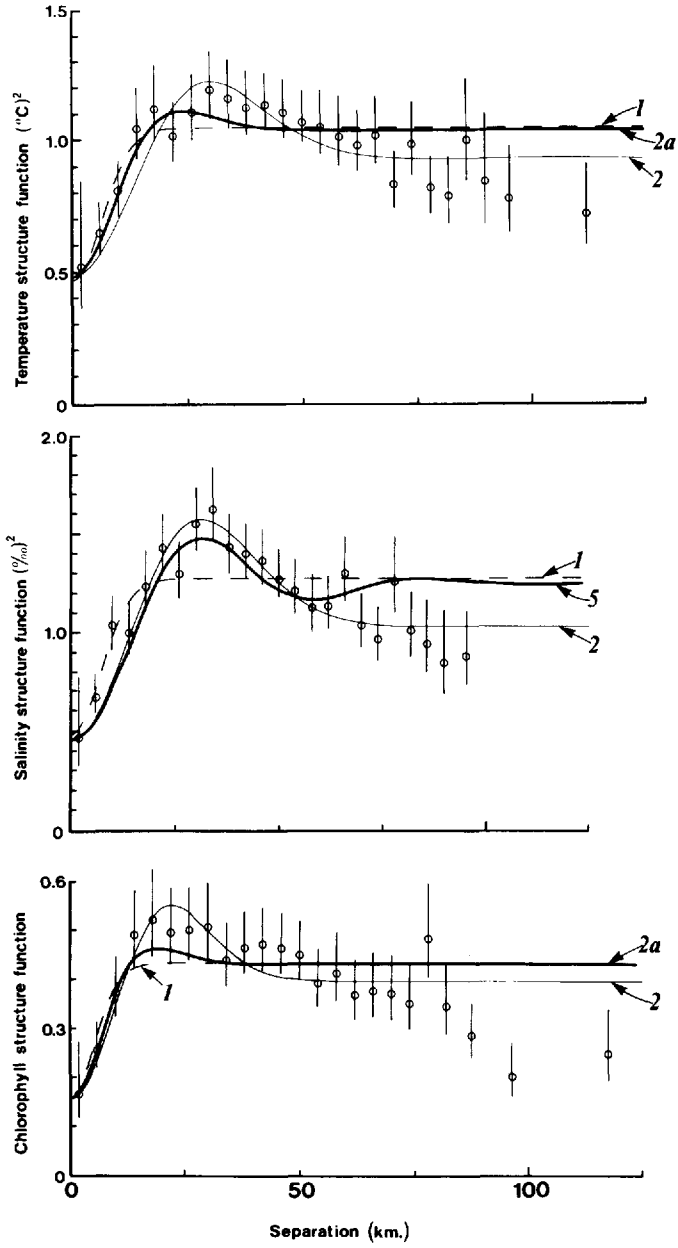

Figure 4. Spatial structure functions of temperature and salinity (0–5 m averages), and phytoplankton chlorophyll *a* pigment (averaged over 0–50 m and $\log_{10}$-transformed). Fitted functions and confidence bars are as in Figure 2.

Kahru *et al.* (1981) also found that on the 10 km scale, depth-integrated chlorophyll concentration was highly correlated with the thickness of a temperature minimum layer just below a warm surface layer in the Baltic Sea.

The structure functions of all three variables contain greater unresolved noise (the asymptote as $r \rightarrow 0$) than does that of geopotential height. A partial explanation is that we calculated these structure function estimates from near-surface data. In addition, the chlorophyll structure function estimates are calculated from a much smaller data set, chlorophyll is derived from fluorescence by means of a relationship that varies both in space and time, and the time scale for significant growth or mortality of phytoplankton ($\simeq$1 day) is small relative to both the duration of a survey and the lifetime of an eddy.

There are, however, more fundamental reasons for expecting differences between structure functions of these scalar fields and of geopotential height. In two-dimensional turbulent flow, the velocity field, the vorticity field, and advected scalar fields all involve multiple spatial derivatives of the streamfunction field, e.g. Eq. (4), operations that result in enhancement of small scale structure. Also, according to spectral theory, the wavenumber spectra of vorticity and passive scalars have proportionately much greater variance at small scales than the spectrum of the streamfunction (e.g. Lesieur *et al.*, 1981). The implication is that the sampling scheme for velocities and for dynamically passive scalar tracers such as chlorophyll must resolve a significantly shorter spatial scale than that which is adequate for the mapping of geopotential height fields.

4. Objective maps

The structure function estimates from observations have provided us with several forms for $F(r)$ and with values for E. What do objective maps constructed with these functions look like, and how sensitive are the maps to different $F(r)$ and E? In the maps presented, we have used the Gauss-Markov theorem to interpolate the data from each survey onto a 4 km rectangular grid and then calculated the crossings of the contour lines at the edges of the 4 km boxes by simple linear interpolation. The Gauss-Markov interpolation was applied on residual data after a fitted (x, y) plane was removed, but the plane was added back to the interpolated residuals before contouring. Expected squared errors were calculated at each grid point, and contours were drawn only where the expected squared error was less than 50% of the signal variance; i.e., where $\langle(\hat{\theta} - \theta)^2\rangle / \langle\theta^2\rangle < 0.5$.

In Figure 5 are four different objective maps for the geopotential height between 50 and 100 m depths for a cruise in June 1981. Panel (a) employs R_1 with the fitted value $a = 15.3$ km. There are gaps in the contours where the relative squared error is greater than 50%. Panel (b) shows the corresponding map for the interpolated departures from the (x, y) plane before the plane is added back to the objectively derived values. Panel (c) is the map calculated with the best realizable fitted function R_5. Note the larger

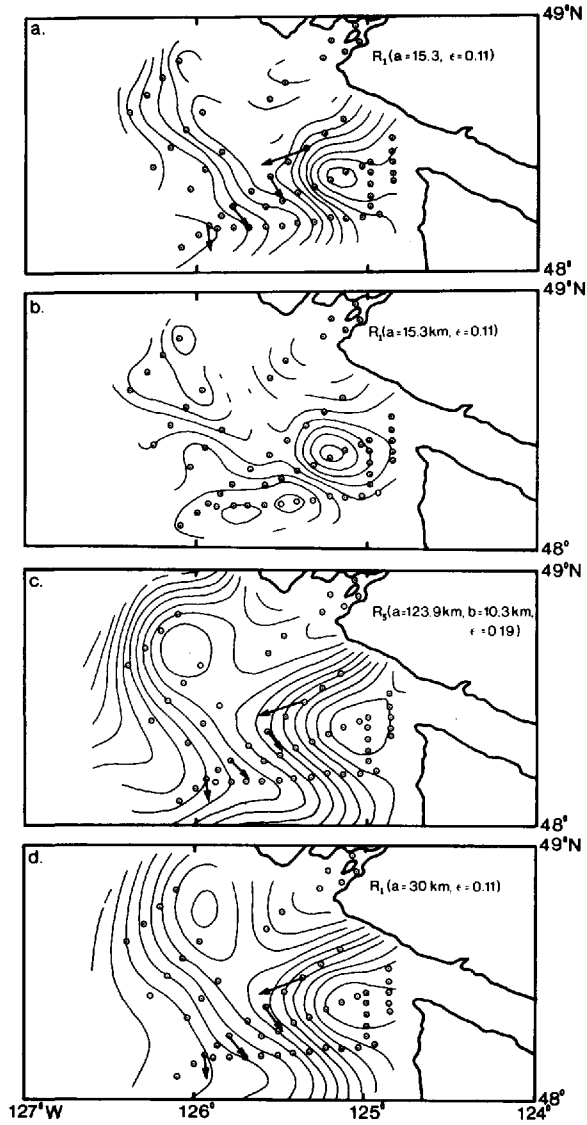

Figure 5. Objectively drawn contour maps of geopotential height between 50 and 100 m for a cruise in June 1981, constructed using the correlation functions with scaling lengths and noise levels $\epsilon = E/F$ (0) as indicated in each panel. Panel (b) is the contoured field of interpolated residuals before the fitted (x, y) plane is added back to produce the map in panel (a). The vectors represent vertical current shear between 50 and 100 m measured from moorings. See text for details.

area over which the function R_5 allows values to be interpolated with a relative squared error less than 50%. This function is less strongly damped, implying correlation at greater separations and therefore greater ability to interpolate from distant observations. R_1 is not a good fit to the data and no doubt underestimates the separations at which significant correlation exists. Are the maps, however, sensitive to the shape of R_5 or only to the increased spatial correlation? A more appropriate value for a in R_1 might be the value that gives the same decay length scale as the function that best fits the structure function estimates, where the decay length scale for functions with zero crossings is calculated as suggested by Lumley (1970):

$$L_u = \int_0^\infty | R(r) | \, dr. \tag{5}$$

We first calculated L_u for the R_i that was the best fit for each variable, and then calculated the value of a that gave the same value of L_u for R_1. For geopotential height, temperature, salinity and log-transformed chlorophyll respectively, we obtained values for a of 33, 30, 41 and 22 km. We then constructed for geopotential height the map plotted in panel (d) of Figure 5 using R_1 with $a = 30$ km, twice that used in the map in panel (a). Differences between the maps in panels (c) and (d) are so small that the required doubling in computation time to use R_5 does not seem warranted. The arrows in Figure 4 represent shear vectors from current meters, filtered with the Lanczos-cosine filter, and evaluated at the central time for the period during which the CTD stations along the line of moorings had been occupied.

In Figure 6 we have plotted objective maps of temperature, salinity and log-transformed chlorophyll for a cruise in April–May 1981. We have used R_1 with $a = 30$ km for temperature and geopotential height and $a = 22$ km for chlorophyll, and with noise (or zero separation variance) values $\epsilon = E/F(0)$ estimated from Figures 2 and 4. In panel (d), we have replotted the map in panel (c) with the noise value reduced to 0.11, the same as for geopotential height in Figure 5. The smaller correlation length scale for chlorophyll causes some contours to be truncated (at 50% relative expected squared error) closer to the observation points. The differences between panels (c) and (d) are that the contours in (d) are somewhat distorted by being constrained to fit the observations more closely because of the much lower assumed noise level, and that the maximum value within the major eddy is greater for the same reason. The pattern itself is relatively unchanged by the lower noise level.

5. Temporal structure functions

During the 25 cruises over the 3-year period, several lines of stations ($\simeq$10 stations to a line) running across the shelf were repeated on different cruises and occasionally on the same cruise. We have calculated, for any 2 occupations of the same station line, a temporal structure function estimate from all pairs of common stations. The time lag is taken as the average of the time lags between station pairs, and weighted average

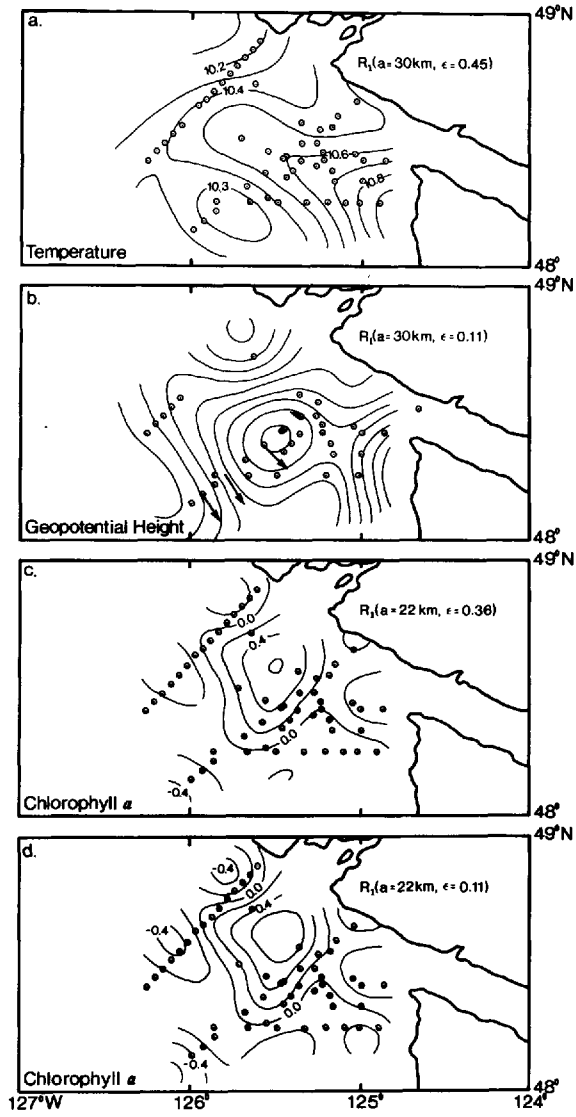

Figure 6. Objectively drawn contour maps of temperature, geopotential height, and $\log_{10}$-transformed chlorophyll for a cruise in April–May 1981. Details are the same as for Figure 5.

estimates have been formed for time lag bins (the first 36.5 days wide, each of the rest 73 days wide). No trends were removed in either space or time.

The results for geopotential height (between 50 and 100 m), temperature and salinity (both 0–5 m) are plotted in Figure 7; the time lag is also a bin-weighted average. Relative 95% confidence limits were calculated as in Figures 2 and 4 for a χ^2 variable with $n - 1$ degrees of freedom (n is the numbers of pairs of stations in the bin), without reducing the df to account for covariability over time. An annual cycle appears in the structure functions of geopotential height and temperature, and to a lesser extent of salinity, for lags up to about 2 years, but there are insufficient data to remove a fitted annual cycle and consider random residuals about that cycle.

In all 3 variables, the structure functions increase in magnitude with time lag up to 6 months. Can we extrapolate this trend backward down to lags comparable with the time taken for one ship survey ($<$ 1 week) to test the validity of our assumption (implicit in our procedure for the estimation of spatial structure functions) that the horizontal patterns change relatively little during a survey? We have replotted in Figure 8 the data from Figure 7 in time lag bins of 1–10, 10–30, 30–50, 50–70, and 70–90 days. If the temporal structure function estimate for time lags of 10 days or less is significantly less than twice the average signal variance for a survey, then spatial patterns inferred from a survey are greater than changes that occur during the survey, and the objective mapping should yield meaningful patterns. (The asymptotic values at large lags in Figures 2 and 4 are not appropriate because the fitted (x, y) planes have removed much of the large scale variance.) For geopotential height, temperature and salinity respectively, the ratios of the first point in Figure 8 to twice the average survey variance are 0.136, 0.544 and 0.072. Only for temperature are the temporal changes over 10 days or less comparable with observed spatial variances. But even then the spatial patterns have twice the variance, which should allow meaningful maps to be constructed. Possibly temperature patterns change more rapidly than salinity patterns on scales of hours to days because near-surface temperature is less conservative at those time scales due to modification by local heat and radiative exchanges. This lack of conservation is reflected in the noise variable E, which was close to half the asymptotic spatial variance for both temperature and chlorophyll (Fig. 4). The spatial patterns of these variables were characterized by fronts, especially in late summer, which contribute to this high error variance and are difficult to map accurately by objective techniques.

6. Discussion

The spatial structure functions of all variables have a peak near separations of 30 km which was not apparent in structure functions calculated before linear trends were removed. If the peak is not an artifact of the trend removal, then it represents a dominant length scale of $\simeq$60 km (in analogy with the first minimum in a covariance function). In fact, during the summer months, a stationary eddy of similar dimension

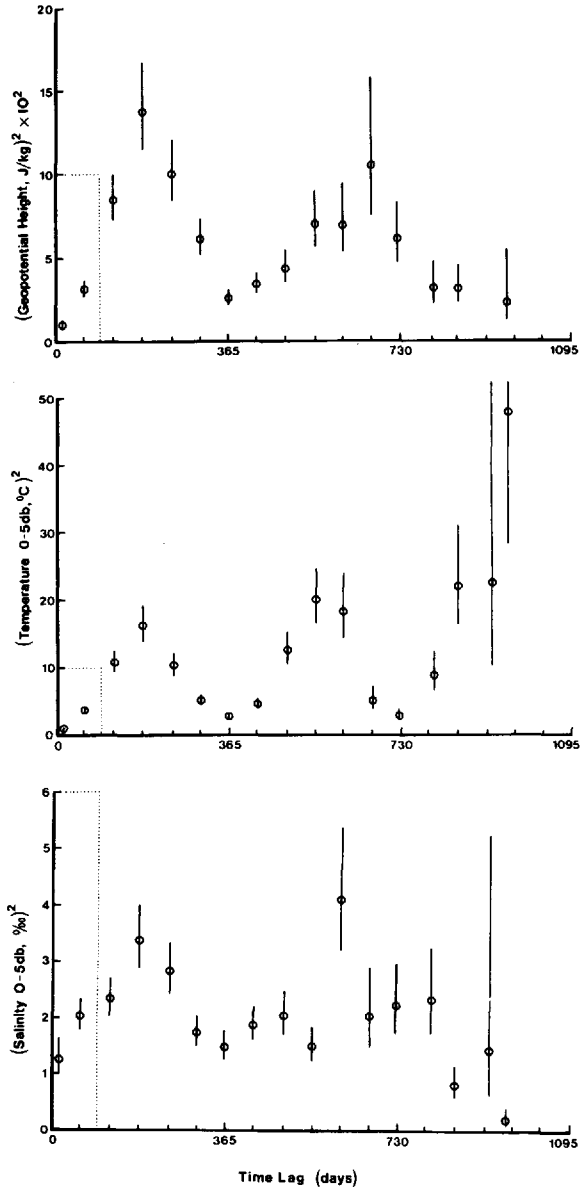

Figure 7. Temporal structure functions of geopotential height, temperature and salinity from lines of CTD stations repeated on different cruises. The position of each point along the axis of time separation represents a bin-weighted average separation, and the bars represent relative 95% confidence intervals for χ^2 variables. The dotted areas are expanded in Figure 8.

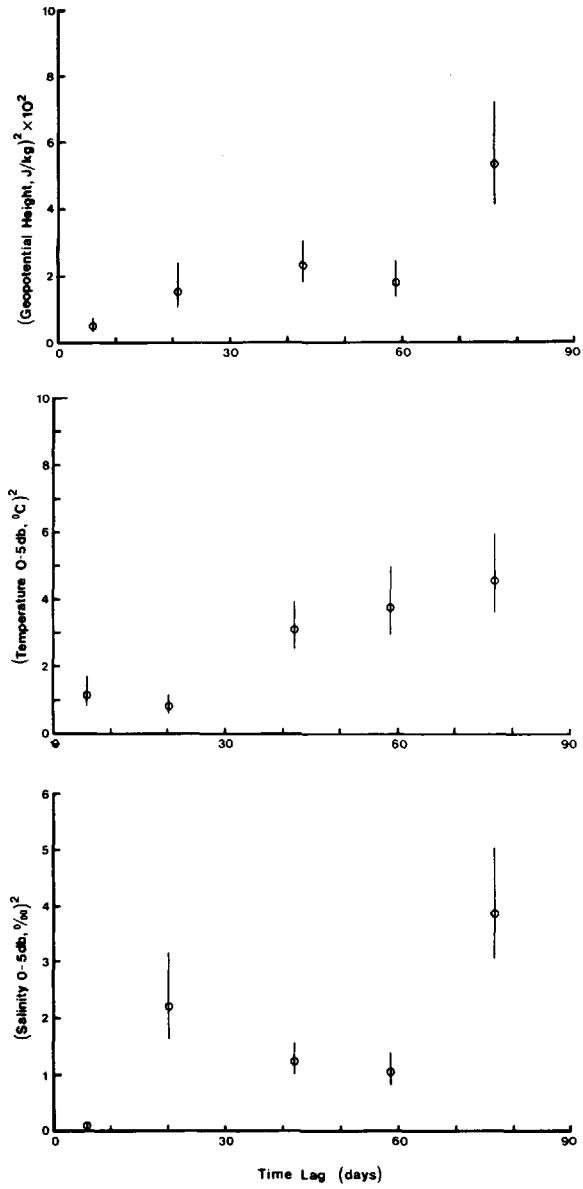

Figure 8. An expanded plot of Figure 7 for small time separations.

was usually present in all the variables at depths of 50 m and below (Freeland and Denman, 1982). Although the eddy was not usually visible in near-surface temperature measurements (Borstad *et al.*, 1982 and Fig. 6), the structure functions for temperature, salinity, and chlorophyll display the same maximum (Fig. 4). In addition, while the eddy was present only during summer months, separate structure functions of geopotential height calculated for summer and winter had roughly the same shape. Thus, temporally varying or horizontally propagating eddy patterns with a wavelength of order 60 km were likely present during most cruises to cause the peak in structure functions, an interpretation similar to that of Mackas (1984) based on spatial autocorrelations of plankton community composition calculated from data obtained on a subset of the cruises discussed in this paper.

What might be the source or generating mechanism for these eddies? The prevailing currents over the continental slope off Vancouver Island are frequently baroclinically unstable, especially during late summer, with eddies or meanders growing initially with wavelength 50–100 km and which eventually distort the flow over the continental shelf (Thomson, 1984; Ikeda *et al.*, 1984). Once perturbed, could the density field over the shelf support baroclinic waves or meanders at these wavelengths?

We can estimate the length of the fastest growing baroclinic wave for the area on the shelf from Eady's (1949) flat bottom model as discussed by Pedlosky (1979). The model considers mean zonal flow but the inertial frequency f is constant, which is quite acceptable for the relatively small north-south scales considered here and which also allows a mean flow in any direction. The wavelength for maximum growth is given as $\lambda = g(S, L_d)L_d$ where g is a function of the internal Rossby radius of deformation $L_d = ND/f$ and a stratification parameter $S = L_d^2/L^2$. N is a mean buoyancy frequency, D is water depth, and L is the horizontal scale of the flow. For baroclinic instability we require $S < O(1)$; g varies gradually between 3.92 and 4.98 for $0 \leq S \leq 1$. The Rossby radius L_d is plotted in Figure 9 for a station near the shelf break. There is a seasonal cycle in L_d between 10 and 20 km, with a mean of 16 km. Taking for L the shelf width ($\simeq$60 km), we get $S = 0.071$ and $g = 4.0$ giving the wavelength of the fastest growing baroclinic wave as $\lambda = 64$ km. In summer this value would be closer to 80 km, suggesting that the flow on the shelf would be receptive to distortion by the lowest mode meander on the slope observed and modelled by Ikeda *et al.* (1984). It must be emphasized that this wavelength, consistent with that inferred from the shape of the structure function, is only valid as an order of magnitude estimate. A model for baroclinic instability with continuous stratification for a specified coastal geometry is required, but as our sampling region occurs at the boundary between the Vancouver Island shelf (oriented NW-SE, relatively broad, and irregular) and the Washington-Oregon shelf (oriented N-S, narrow, and regular), there is no single simple choice of shelf geometry for such a model.

While we can infer from the spatial structure functions a dominant spatial scale for horizontal pattern in the sampling region, the temporal structure functions resolve only an annual cycle, already observed in time series of both hydrographic properties

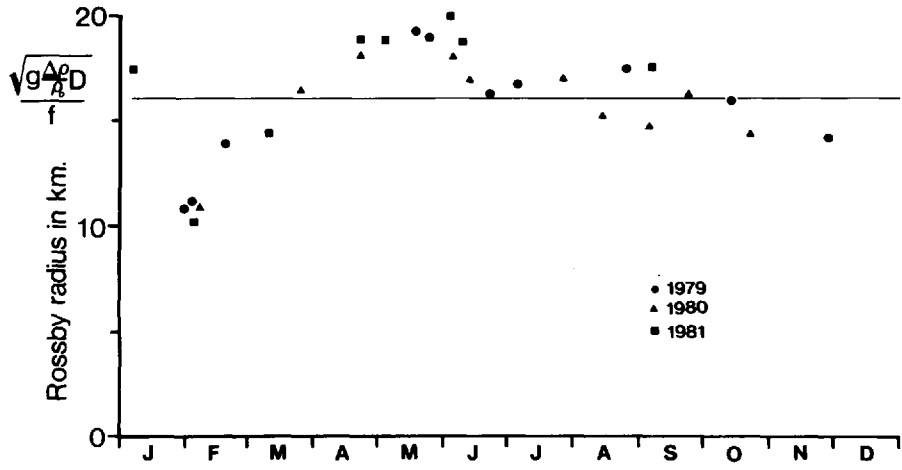

Figure 9. The annual cycle in the internal Rossby radius of deformation at a shelf edge CTD station (near the mooring location just outside the 100 fm contour shown in Fig. 1). The horizontal line represents the mean value.

(Freeland and Denman, 1982) and currents (Freeland *et al.*, 1984). Can we estimate a time scale associated with patterns of characteristic wavelength ≃60 km?

During our experiment, a mooring was maintained in just over 200 m of water near the shelf break (the vector located just outside the 100 fm contour in Fig. 1) for over 3 years with current meters at depths of 50, 100 and 200 m. We have constructed a composite kinetic energy spectrum for the current at 50 m from several analyses of progressively filtered data but with overlap between the separate spectra (shown in Fig. 10). There appear to be 3 bands of elevated energy levels: one centered on the annual period, a possible plateau between 50 and 10 day periods followed by a constant slope subrange at shorter periods, and a band of several peaks between periods of 24 and 12 hours (K_1—diurnal, f—inertial, and M_2—semidiurnal) followed by another subrange at even shorter periods out to the Nyquist period of 2 h. We suggest that the middle band between 50 and 10 days represents the energy associated with eddy patterns with wavelengths ≃60 km. That band is displayed more convincingly in Figure 11 plotted on variance-conserving axes. In this figure, there is a clear peak in the energy spectrum at a period of 20 days with a cascade region falling off at shorter periods and a distinct gap separating it from the annual peak at longer periods. The spectrum for the current meter at 100 m depth was indistinguishable from the one for 50 m plotted in Figure 11, indicating that over much of the water column at the shelf edge, mesoscale fluctuations with a period centered on 20 days accounted for a significant fraction (≃30%) of the total kinetic energy in the horizontal currents. Both Thomson (1984) and Ikeda *et al.* (1984) calculated a characteristic lifetime for baroclinic eddies over the continental slope of ≃25 days.

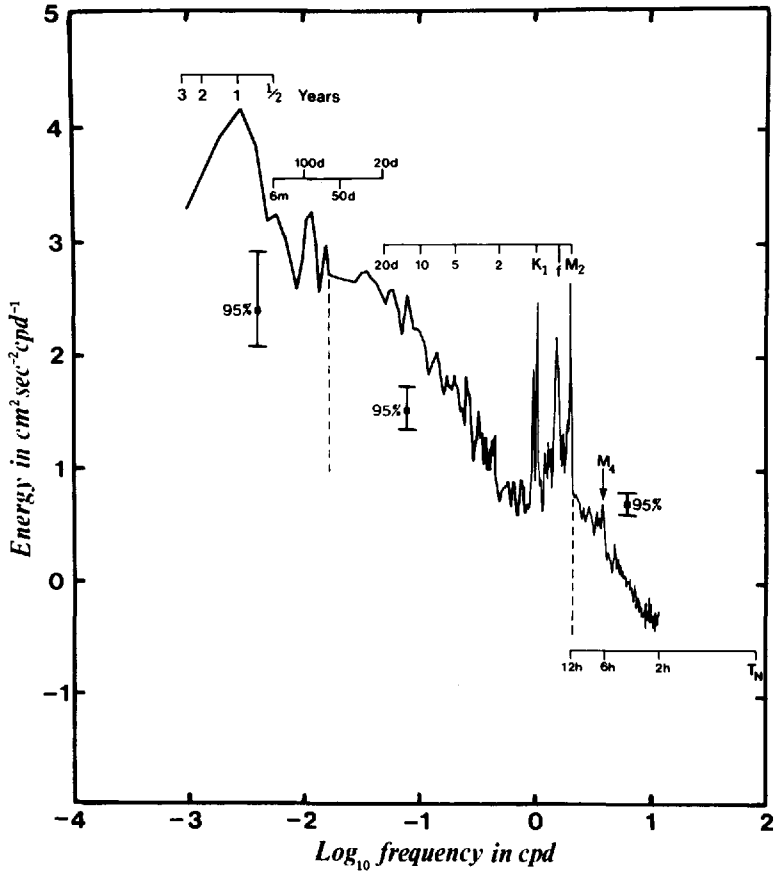

Figure 10. A composite kinetic energy spectrum on a log-log scale of current at 50 m from the shelf edge mooring shown in Figure 1, constructed from several analyses of the data, but with overlap between the separate spectra.

7. Summary

We have estimated spatial and temporal structure functions from synoptic ship survey data and moored current meter data obtained over a 3-year period (1979–81) from the continental shelf off Vancouver Island, Canada. The data were insufficient to resolve the anisotropy and inhomogeneity known to exist over continental shelves. Reasonable agreement was obtained between longitudinal and transverse structure function estimates calculated from measured currents and estimates derived from the hydrographic data, indicating that the assumption of quasi-geostrophic flow was not strongly violated. In addition, observed low-pass filtered shear measurements from current meters agreed well with flows inferred from the objectively-derived maps of geopotential height. The shape of the spatial structure functions of geopotential height,

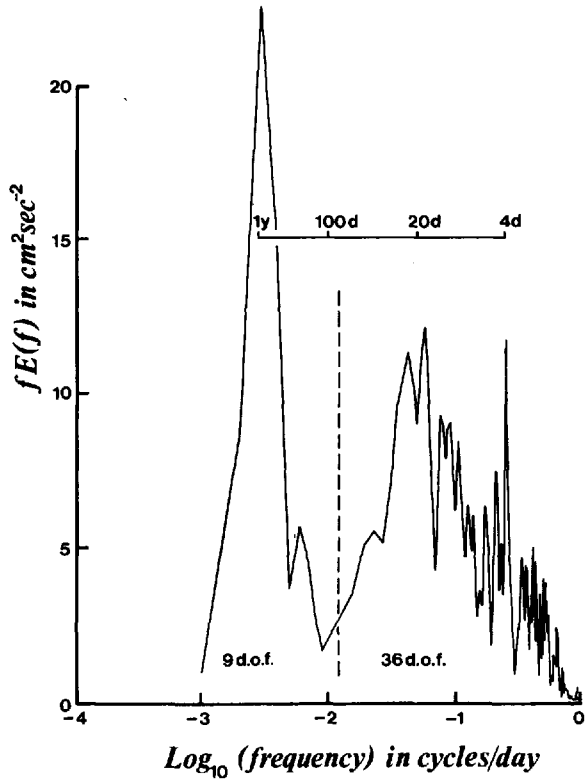

Figure 11. The kinetic energy spectrum of current from Figure 10 replotted on energy-preserving axes to show the gap between the annual and mesoscale peaks in energy. We have filtered out the diurnal and higher frequency signal energy.

temperature, salinity and to a lesser extent log-transformed depth-integrated derived chlorophyll *a* pigment concentration implied horizontal patterns with a characteristic wavelength of ≃60 km. The temporal structure functions resolved a periodicity only at the annual cycle, but the spectrum from a long term current meter record had a peak between 10 and 30 day periods probably associated with the eddy structure, as well as peaks at the annual period and at the dominant tidal and inertial periods.

Objective maps of two surveys were constructed using different correlation functions and error (or noise) levels obtained from the structure function estimates. The maps were relatively insensitive to both the form of the correlation function $R(r)$ and the squared noise level E, but the higher noise levels in the near-surface variables (due to more small scale structure and to temporal change during individual surveys) decreased the confidence in the patterns depicted in individual maps. The maps do generate believable patterns, and the evolution of the patterns during the course of a

survey appears to be small enough to be acceptable statistically. However, the objective mapping technique used here will not replicate the streakiness of scalar tracer fields in geostrophic turbulence, observed both from satellites and in numerical simulations (e.g., Denman and Powell, 1984; Holloway and Kristmannsson, 1984). To determine how much the patterns are undersampled by ship survey and how much they evolve during the course of a survey, careful analysis of series of satellite images by similar techniques is required.

Acknowledgments. We thank the officers and crews of the Canadian research ships *Parizeau, Vector* and *Endeavour* for their cooperation and assistance, and all those who provided technical assistance, especially S. Hill and A. Stickland. W. Crawford supplied current meter data from the two northern moorings. We also acknowledge helpful comments from P. Budgell, D. Chelton, R.O.R.Y. Thompson, R. E. Thomson and three referees; and financial support from the U.S. National Aeronautics and Space Administration Oceanic Processes Program under grant number NAG 5-217. Finally, we wish especially to thank our colleagues A. Bennett and D. Mackas for their continued comments and encouragement.

REFERENCES

Alaka, M. A. and R. C. Elvander. 1972. Optimum interpolation from observations of mixed quality. Mon. Wea. Rev., *100,* 612–624.

Bennett, A. F. and K. L. Denman. 1985. Phytoplankton patchiness: inferences from particle statistics. J. Mar. Res., *43,* 307–335.

Bevington, P. R. 1969. Data Reduction and Error Analysis for the Physical Sciences. McGraw-Hill, New York, 336 pp.

Borstad, G. A., R. M. Brown, D. Truax, T. R. Mulligan and J. F. R. Gower. 1982. Remote sensing techniques for fisheries oceanography: examples from British Columbia. NAFO Sci. Coun. Studies, *4,* 69–76.

Bretherton, F. P., R. E. Davis and C. B. Fandry. 1976. A technique for objective analysis and design of oceanographic experiments applied to MODE-73. Deep-Sea Res., *23,* 559–582.

Bretherton, F. P. and J. C. McWilliams. 1980. Estimations from irregular arrays. Rev. Geophys. Space Phys., *18,* 789–812.

Cassie, R. M. 1963. Microdistribution of plankton. Oceanogr. Mar. Biol. Ann. Rev., *1,* 223–252.

Denman, K. L. and T. M. Powell. 1984. Effects of physical processes on planktonic ecosystems in the coastal ocean. Oceanogr. Mar. Biol. Ann. Rev., *22,* 125–168.

Eady, E. T. 1949. Long waves and cyclone waves. Tellus, *1,* 33–52.

Freeland, H. J., W. R. Crawford and R. E. Thomson. 1984. Currents along the Pacific coast of Canada. Atmos.-Ocean, *22,* 151–172.

Freeland, H. J. and K. L. Denman. 1982. A topographically controlled upwelling center off southern Vancouver Island. J. Mar. Res., *40,* 1069–1093.

Freeland, H. J. and W. J. Gould. 1976. Objective analysis of meso-scale ocean circulation features. Deep-Sea Res., *23,* 915–923.

Gandin, L. S. 1965. Objective Analysis of Meteorological Fields. Israel Program for Scientific Translations, Jerusalem, 242 pp.

Holloway, G. and S. S. Kristmannsson. 1984. Stirring and transport of tracer fields by geostrophic turbulence. J. Fluid Mech., *141,* 27–50.

Ikeda, M., L. A. Mysak and W. J. Emery. 1984. Observation and modelling of satellite-sensed meanders and eddies off Vancouver Island. J. Phys. Oceanogr., *14,* 3–21.

Kahru, M., A. Aitsam and J. Elken. 1981. Coarse-scale spatial structure of phytoplankton standing crop in relation to hydrography in the open Baltic Sea. Mar. Ecol. Prog. Ser., *5,* 311–318.

Karweit, M. 1980. Optimal objective mapping: a technique for fitting surfaces to scattered data, *in* Advanced Concepts in Ocean Measurements for Marine Biology, F. Diemer, F. Vernberg and D. Mirkes, eds., Univ. South Carolina, Columbia, 81–99.

Kendall, M. and A. Stuart. 1979. The Advanced Theory of Statistics, Vol. 2, Inference and Relationship. Macmillan, New York, 748 pp.

Lesieur, M., J. Sommeria and G. Holloway. 1981. Zones inertielles du spectre d'un contaminant passif en turbulence bidimensionelle. C. R. Acad. Sc. Paris, *292(II),* 271–274.

Lilliefors, H. W. 1967. On the Kolmogorov-Smirnov test for normality with mean and variance unknown. J. Amer. Statist. Ass., *62,* 399–402.

Lumley, J. L. 1970. Stochastic Tools in Turbulence. Academic Press, New York, 194 pp.

Mackas, D. L. 1984. Spatial autocorrelation of plankton community composition in a continental shelf ecosystem. Limnol. Oceanogr., *29,* 451–471.

McWilliams, J. C. 1976. Maps from the Mid-Ocean Dynamics Experiment: Part I. Geostrophic streamfunction. J. Phys. Oceanogr., *6,* 810–827.

Monin, A. S. and A. M. Yaglom. 1975. Statistical Fluid Mechanics: Mechanics of Turbulence, Vol. 2. MIT Press, Cambridge, MA., 874 pp.

Mood, A. M. and F. A. Graybill. 1963. Introduction to the Theory of Statistics, McGraw-Hill, New York, 443 pp.

Pedlosky, J. 1979. Geophysical Fluid Dynamics. Springer-Verlag, New York, 624 pp.

Smith, R. C. and K. S. Baker. 1982. Oceanic chlorophyll concentrations as determined by satellite (Nimbus-7 Coastal Zone Color Scanner). Mar. Biol., *66,* 269–279.

Stommel, H. 1963. Varieties of oceanographic experience. Science, *139,* 572–576.

Thomson, R. E. 1984. A cyclonic eddy over the continental margin of Vancouver Island: evidence for dynamical instability. J. Phys. Oceanogr., *14,* 1326–1348.

Yaglom, A. M. 1962. An Introduction to the Theory of Stationary Random Functions. Prentice-Hall, New York, 235 pp.

Received: *21 March, 1984;* revised: *12 April, 1985.*